J. Fluid Mech. (2006), *vol.* 552, *pp.* 381–392.
doi:10.1017/S002211200600872X Printed in the United Kingdom

Critical flow solution to Gill's model of rotating channel hydraulics

By R. IACONO

ENEA, C.R. Casaccia, Via Anguillarese 301, Rome, Italy

(Received 22 March 2005 and in revised form 28 September 2005)

Gill's semigeostrophic equations of one-layer, rotating channel hydraulics are exactly solved at the critical section, for flows with a finite uniform potential vorticity (PV). A detailed characterization of the critical flow at the sill is consequently obtained, together with a simple, explicit expression for the associated mass transport, that provides a direct extension of the well-known transport formula of zero-PV theory.

The dependence of the mass transport on the PV, for a given average flow energy, is found to be non-monotonic. In particular, the transport increases when the PV is raised from zero, attaining a maximum value that can be up to twice those predicted by the zero-PV theory. This suggests that, contrary to common belief, finite-PV effects may be important in determining the mass transport in real oceanic outflows.

1. Introduction

In spite of their limitations, single-layer, reduced-gravity models have proven very useful in the characterization of real oceanic ouflows, providing the basis for most of the analytic understanding achieved in the field. Reference steady models are that of Whitehead, Leetma & Knox (1974, referred to as WLK hereafter), that assumes zero potential vorticity (PV), and the model by Gill (1977), that allows for a finite, uniform PV. The former model leads to a simple formula for transport in a critical flow, which has often been used to obtain 'zeroth-order' estimates of the mass flux in oceanic straits that are believed to be hydraulically controlled (see e.g. Whitehead 1989, 1998). A corresponding formula for the finite-PV case is lacking, since in its usual formulation the Gill model leads to high-order algebraic equations, that prevent an analytic characterization of the flow.

A common statement about transport in finite-PV theory is that it is generally smaller than that predicted by the WLK formula. The origin of this belief can be traced back to works by Shen (1981) and Whitehead (1989), that show, among other things, a weakly decreasing dependence of transport on PV. Those works, however, explored a limited range of parameters, and so the generality of the conclusions on transport they have prompted might be questionable. Besides, there appears to be no clear physical reason why a finite PV should lead to a decrease of the mass transport.

In the present work, we shall gain further insight into the effect of a finite PV, by exploiting the fact that, for an appropriate choice of the upstream flow invariants, the semigeostrophic equations can be exactly solved at the channel sill. This allows us to give an analytic characterization of attached and detached critical flows at the sill, and to derive simple, exact expressions for the associated mass transports. These expressions directly extend the WLK formulae to flows with a finite PV, and point to a richer range of behaviours than previously thought.

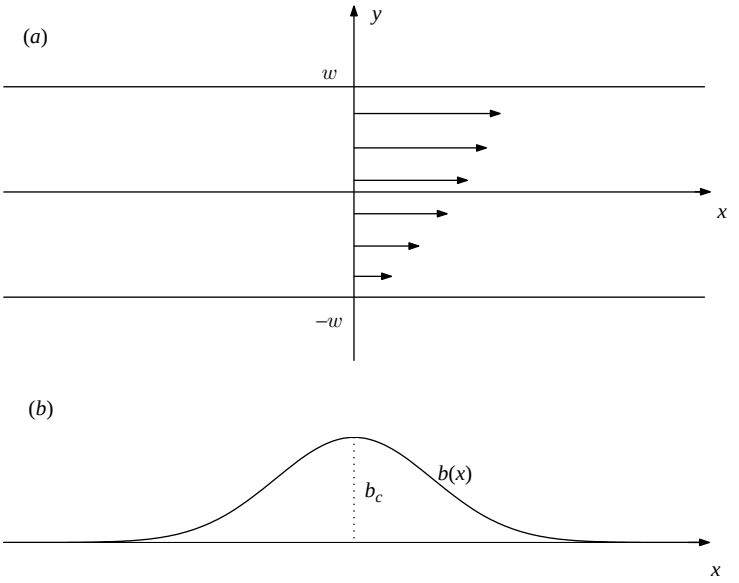

FIGURE 1. Sketch of the problem geometry: (*a*) a top view of the channel, showing the chosen (x, y) coordinate system, with the x-axis pointing downstream; (*b*) a side view of the bottom topography, which only varies along x. The wall at $y = -w$ ($y = w$) is denoted as eastern (western) throught the paper, following a notation by Killworth (1992). Values at the eastern (western) wall are denoted by a minus (plus) subscript.

The paper is organized as follows. Section 2 gives the basic equilibrium equations. In § 3, these equations are explicitly solved at the sill for a critical flow, and the solutions are analysed in a normalized energy–PV space, in which different flow regimes are easily identified. Exact expressions for the corresponding mass transports are then derived in § 4, while the main results are summarized and further discussed in § 5.

2. Basic equations

We consider steady, reduced-gravity shallow-water flows, in a rectangular, rotating channel, bounded by rigid walls at $y = \pm w$ (figure 1 gives a sketch of the problem geometry, together with related definitions). The semigeostrophic approximation is assumed to hold (see Gill 1977 and Pratt 1983 for details). As a consequence, the equilibrium problem reduces to a single second-order PDE for the fluid depth h,

$$\frac{g}{f}\frac{\partial^2 h}{\partial y^2} - qh = -f, \tag{2.1}$$

where f is twice the rotation frequency, g the reduced gravity, and q the constant, positive PV value. Integration of (2.1), and use of geostrophic balance, yields expressions for h and for the along-channel velocity u, that we write as

$$\frac{u}{\sqrt{gH}} = \frac{1}{C}\left[\left(1 - \frac{\bar{h}}{H}\right)\sinh(y/L_R) + \frac{\bar{u}}{\sqrt{gH}}\cosh(y/L_R)\right], \tag{2.2}$$

$$\frac{h}{H} = 1 - \frac{1}{C}\left[\frac{\bar{u}}{\sqrt{gH}}\sinh(y/L_R) + \left(1 - \frac{\bar{h}}{H}\right)\cosh(y/L_R)\right]. \tag{2.3}$$

Here $H \equiv f/q$, $L_R \equiv \sqrt{gH}/f$ is the Rossby deformation radius associated with H, $C \equiv \cosh(w/L_R)$, and the two free functions of x resulting from the integration of (2.1) have been expressed in terms of the averages $\bar{u}$ and $\bar{h}$ (unless otherwise specified, here we adopt the notation $\bar{F} \equiv (F^+ + F^-)/2$, and $\Delta F \equiv F^+ - F^-$). Evaluating (2.2)–(2.3) at the walls, we compute

$$\Delta h = -\left(\frac{H}{g}\right)^{1/2} 2T\bar{u}, \tag{2.4}$$

$$\bar{h} = H - \left(\frac{H}{g}\right)^{1/2} \frac{1}{2T}\Delta u, \tag{2.5}$$

where $T \equiv S/C$, $S \equiv \sinh(w/L_R)$. Note that if $\Delta u = 0$, $\bar{h}$ $(= H)$ is the depth at $y = 0$. The corresponding velocity (depth $-H$) field is symmetric (antisymmetric) with respect to $y = 0$. On the other hand, $\bar{h} < H$ if $\Delta u > 0$, i.e. if the flow speed is larger at the western wall.

The equilibrium system is closed by expressions for two of the flow invariants: the average Bernoulli function $\bar{B}$,

$$\bar{B} = g\bar{h} + gb(x) + \frac{gH}{2} T^2 \left(1 - \frac{\bar{h}}{H}\right)^2 + \frac{1}{2}\bar{u}^2, \tag{2.6}$$

and the along-channel mass transport Q,

$$Q = 2L_R T \bar{h}\bar{u}. \tag{2.7}$$

For given values of q, $\bar{B}$ and Q, and a given topography $b(x)$, $\bar{u}(x)$ and $\bar{h}(x)$ may be computed from (2.6)–(2.7) by solving a quartic algebraic equation at any x.

In order to determine solutions that correspond to hydraulically controlled flows, one has to free one of the parameters, so that criticality at the sill location may be imposed. This can be done in several ways. In Pratt (1983), for example, the value of the sill height is not prescribed, but determined as a part of the solution, by imposing a semigeostrophic Froude number equal to unity at the sill. Different choices of the flow invariants are made in Gill (1977), and in more recent works by Helfrich & Pratt (2003) and Whitehead & Salzig (2001, referred to as WS hereafter). In all cases, quartic algebraic equations need to be solved to characterize the flow at the critical section. Yet another approach is considered in the next section, which allows us to completely solve the equations at the sill.

3. Solution for a critical flow

We assume a given sill height $b_c = b(x_c)$ and a given $\bar{B}$, leaving the mass transport unspecified. We then impose criticality, by taking ∂_x of (2.6) and (2.7), evaluated at the sill, where $\partial_x b = 0$, and setting to zero the determinant of the coefficient matrix of the resulting linear homogeneous system of equations for $\partial_x \bar{h}|_{x_c}$ and $\partial_x \bar{u}|_{x_c}$. This yields

$$\frac{\bar{u}}{\sqrt{gH}} = \left(\frac{\bar{h}}{H}\right)^{1/2} \left(1 - T^2 + T^2 \frac{\bar{h}}{H}\right)^{1/2}. \tag{3.1}$$

Placing (3.1) in (2.6), evaluated at the sill, and solving the resulting quadratic equation, finally gives $\bar{h}$ in terms of the parameters of the problem:

$$\frac{\bar{h}}{H} = \frac{3}{4S^2}\left(-1 + \sqrt{1 - \frac{8}{9}S^4 + \frac{16}{9}S^2C^2\frac{\Delta z}{H}}\right), \tag{3.2}$$

where $\Delta z \equiv \bar{B}/g - b_c$. Expressions (2.2)–(2.3), together with (3.1)–(3.2), give a complete description of attached critical flows at the sill. It is seen from (3.2) that $\bar{h}/H$ increases monotonically when Δz is increased. Correspondingly (see (2.5)), Δu decreases, vanishes for $\Delta z/H = \Delta z/\bar{h} = 3/2$, and becomes negative for larger values of the energy, yielding a larger flow speed at the eastern wall. We do not know if flows with negative Δu have been experimentally observed.

As shown by Gill (1977), attached flow requires that $h^{\pm} > 0$. Since $\Delta h < 0$ for $\bar{u} > 0$, it is sufficient that $h^{+} > 0$, which, using (2.3) and (3.1), is seen to be equivalent to

$$\frac{\bar{h}}{H} > \frac{T^2}{1+T^2}. \tag{3.3}$$

Using (3.2), this translates into

$$\frac{\Delta z}{H} > 1 - \frac{1}{(1+T^2)^2}. \tag{3.4}$$

Condition (3.4) corresponds to the existence of a threshold in $\bar{B}$ above which solutions are attached to both walls. For lower values of the energy, solutions are detached from the western wall, and a separate treatment is required (see § 3.1).

The information about critical flow solutions we have gained may be further organized by noticing that these solutions only depend on the two non-dimensional quantities $\Delta z/H$ and w/L_R. This suggests the introduction of the following normalized energy and PV:

$$\Delta z^* = \frac{\Delta z}{w^2 f^2/g}, \qquad q^* = \frac{q}{g/(w^2 f)}, \tag{3.5}$$

in terms of which

$$\frac{\Delta z}{H} = \Delta z^* q^*, \qquad \left(\frac{w}{L_R}\right)^2 = q^*. \tag{3.6}$$

As shown in figure 2, different flow regimes are easily identified in the $(\Delta z^*, q^*)$ space (note that in this space curves of constant $\Delta z/H$ are equilateral hyperbolas). The curve $C1$, approaching the hyperbola $\Delta z/H = 3/4$ (dotted) at large q^*, corresponds to the threshold (3.4); below (above) $C1$ lie critical flows detached (attached) at the sill. On the other hand, the curve $C3$, corresponding to the hyperbola $\Delta z/H = 3/2$, separates flows with $\Delta u > 0$ (below) from those with negative Δu (above). Inside the region between $C1$ and $C3$ another transition occurs, marked by the curve $C2$. This curve separates flows with convex depth profiles (below) from flows with depth profiles that become concave in the eastern part of the channel (above). The transition corresponds to the violation of the condition $h/H \leqslant 1\ \forall y$, which implies both a convex depth profile (see (2.1)) and a monotonically increasing profile of the Froude number $F = u/(gh)^{1/2}$. Above $C3$ one finds attached flow solutions with $\Delta u < 0$, that always have concave depth profiles near the eastern wall and tend to develope non-monotonic profiles of F.

Explicit solutions, for flows with $\Delta z^* = 1.5$ and $q^* = 0.2, 0.5, 0.9$, and 1.4, are shown in figure 3. The value $q^* = 0.2$ corresponds to a flow just beyond the attached flow

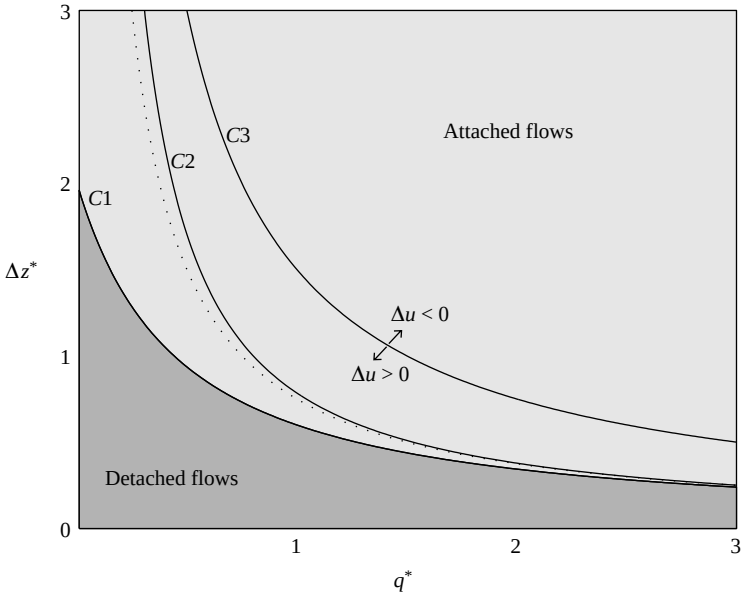

FIGURE 2. Normalized energy(y)–PV(x) diagram for flow solutions at the critical section. The curves $C1$–$C3$ correspond to transitions in flow properties that are detailed in the text.

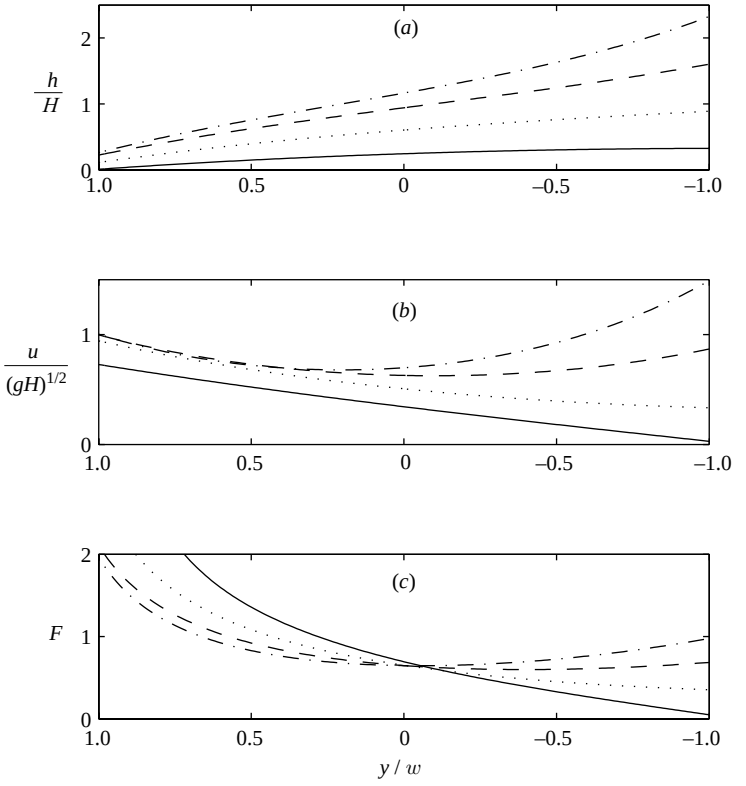

FIGURE 3. Profiles of (*a*) h/H, (*b*) $u/\sqrt{gH}$, and (*c*) F, at the sill section, for attached critical flows with $\Delta z^* = 1.5$ and $q^* = 0.2$ (solid), 0.5 (dotted), 0.9 (dashed), 1.4 (dot-dashed).

boundary, as is seen both from figure 2 and from the lowest depth profile in figure 3(*a*). On the other hand, $q^* = 0.5$ corresponds to a flow close to the transition marked by the curve $C2$ in figure 2. It is seen from figure 3(*a*) that for this flow $\partial_y^2 h$ is close to zero, and h/H close to unity, near the eastern wall, in agreement with the preceeding analysis. The flow with $q^* = 0.9$ is close to the hyperbola $C3$ in figure 2, and has an almost symmetric velocity profile (see figure 3*b*), while the flow with $q^* = 1.4$ has a negative Δu (top profile in figure 3*b*), as expected. The latter two flows have concave depth profiles in the eastern part of the channel, and non-monotonic F profiles (see figure 3*c*).

To conclude this scrutiny of the attached flow solutions, we notice that condition (3.3), together with (3.1), implies that the flow is unidirectional at the sill, as it should (Gill 1977).

3.1. *Detached flow solutions*

We now consider solutions corresponding to flows that are detached at the sill. These solutions are still quite mysterious objects: although their existence is predicted by the semigeostrophic theory, both laboratory experiments (WLK; Shen 1981; Pratt 1987) and numerical simulations using the full shallow water equations (Pratt, Helfrich & Chassignet 2000) have failed to produce them, for reasons that are not well understood.

As noted by several authors, the basic equations are unaffected by the introduction of a shifted y coordinate that goes from $-w_c$ to w_c, with $2w_c$ the width of the flow at the critical section. Consequently, the attached flow solution previously obtained continues to hold, with w replaced by w_c in the argument of the hyperbolic functions (in particular, we write $T_c \equiv T(w_c)$). An additional constraint is now given by the fact that $h^+ = 0$. As noted in Pratt & Armi (1987), this implies that h^-, $\bar{h}$ and Δh are constant in the detached flow region. Evaluating (2.3) at the eastern wall and using (3.1), gives

$$\frac{\bar{h}}{H} = \frac{T_c^2}{1 + T_c^2}, \tag{3.7}$$

which shows that $\bar{h} < H$, and consequently $\Delta u > 0$ for a detached flow. Placing (3.7) in (3.2) yields

$$\frac{\Delta z}{H} = 1 - \frac{1}{\left(1 + T_c^2\right)^2}, \tag{3.8}$$

which can be used to compute the width of the flow at the critical section, for a given ratio $\Delta z/H$. It follows from (3.7)–(3.8) that

$$\frac{\bar{h}}{H} = 1 - \sqrt{1 - \frac{\Delta z}{H}}. \tag{3.9}$$

Substituting this expression and the corresponding expression for $\bar{u}$ in (2.2)–(2.3) gives the complete detached flow solution at the sill. At this point, however, one should address the realizability of such solutions. Since, according to (3.8), the flow width goes to zero when Δz does, it would seem that the existence of a flow detached at the sill simply requires $\Delta z > 0$, and, consequently, that the whole region below the curve $C1$ in figure 2 may be accessed. As will be shown in the Appendix, this is not always the case. The picture is more complex, and, in some cases, the actual region of the parameter space available to separated flow solutions may be much smaller.

4. Critical transport

Placement of (3.1) in (2.7) yields the mass transport corresponding to the critical flow solution we have derived. In non-dimensional form, this is

$$Q_A^* = \frac{T}{q^{*2}} \left(\frac{\bar{h}}{H} \right)^{3/2} \left(1 - T^2 + T^2 \frac{\bar{h}}{H} \right)^{1/2}, \tag{4.1}$$

with

$$Q_A^* \equiv \frac{Q}{2f^3 w^4 / g}. \tag{4.2}$$

Equation (4.1), with $\bar{h}/H$ given by (3.2), provides a simple, exact expression for the critical transport for attached flows. The right-hand side of (4.1) only depends on q^* and Δz^*, and is clearly a monotonically increasing function of Δz^*. The general dependence on q^* is more difficult to assess, but the small and large q^* behaviours are readily obtained. In the vanishing q^* limit, the argument of the hyperbolic functions is small, so that $C \simeq 1$ and $S \simeq T \simeq q^{*1/2}$. One can then set the last term in (4.1) to unity and expand the square root in (3.2) to recover the zero-PV formula of WLK, which in our notation reads

$$Q_{0A}^* = \left(\tfrac{2}{3}\right)^{3/2} \left[\Delta z^* - \tfrac{1}{2} \right]^{3/2}. \tag{4.3}$$

Note that small q^* may be obtained in three different ways: in the narrow channel limit ($w \to 0$), in the small rotation limit ($f \to 0$), and in the small PV limit ($q \to 0$). We have thus shown that the WLK formula holds in all three limits. This corroborates numerical findings of Borenäs & Pratt (1994) (see their figures 9 and 10), showing that predictions based on zero-PV theory are very close to those of finite-PV theory in the case of very narrow channels. In the limit of large q^*, S and C are both large, $T \simeq 1$, and (4.1) reduces to

$$Q_A \simeq \frac{2g}{f} \bar{h}^2, \tag{4.4}$$

in agreement with previous work ((4.4) can be recovered by taking $T = 1$ in equation (4.2) of Pratt 1983, and taking the normalizations into account). It follows from (4.4) and (3.2) that Q_A^* approximately decays as $1/q^*$ at large q^*.

An expression for transport in detached flows is obtained from (4.1) by replacing T with T_c, and using (3.7) (to eliminate the dependence on T_c) and (3.9). We find

$$Q_D^* = \frac{1}{q^{*2}} \left(1 - \sqrt{1 - \Delta z^* q^*} \right)^2. \tag{4.5}$$

At small q^*, this reduces, as it should, to the corresponding zero-PV, WLK expression,

$$Q_{0D}^* = \tfrac{1}{4} \Delta z^{*2}. \tag{4.6}$$

Since the ratio between (4.5) and (4.6) is a monotonically increasing function of q^*, the effect of finite PV (for Δz^* in the detached flow range) is that of increasing the transport. The maximum ratio Q_D^*/Q_{0D}^* is obtained at the threshold (3.4) (at small Δz^*, this approximately coincides with $\Delta z^* q^* = 3/4$, yielding $Q_D^*/Q_{0D}^* \simeq 16/9$).

To complete the picture, in figure 4 we plot the critical mass transport, normalized with the zero-PV values, as a function of q^*, for $\Delta z^* = 3, 2, 1$, and $1/4$. The two top curves, corresponding to the smaller values of Δz^*, are constructed by using the detached flow expression (4.5) at small values of q^*, and expression (4.1) for values of q^* beyond the transition to attached flow solutions (the two expressions join smoothly

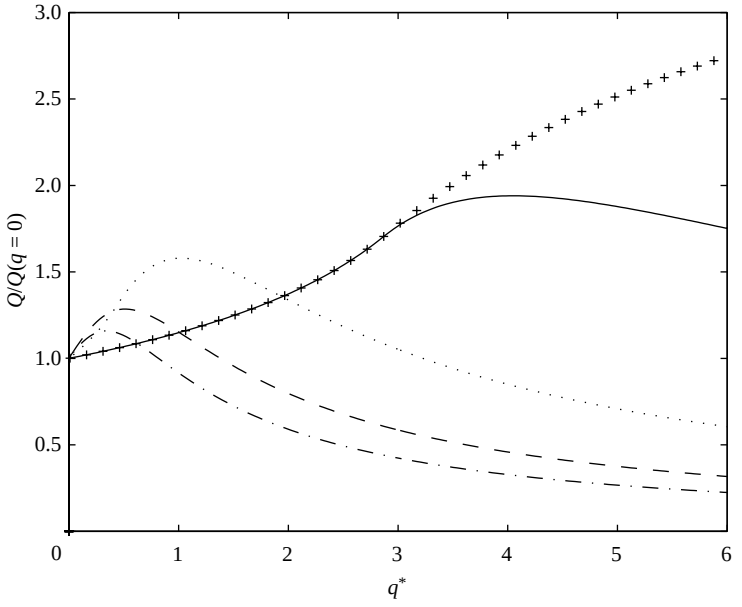

FIGURE 4. Critical mass transport, normalized with the zero-PV values, as a function of q^*, for $\Delta z^* = 1/4$ (solid), 1 (dotted), 2 (dashed), 3 (dot-dashed). Also shown is the transport bound Q_e^*/Q_{0D} given by (5.3) (crosses), for the case $\Delta z^* = 1/4$. The figure shows that transport, for a given Δz^*, is a non-monotonic function of the PV. Transport maxima lie on $\Delta z^* q^* = 1$.

at the transition). The figure shows that the transport increases when q^* is raised from zero, reaches a maximum, and then slowly decreases at larger q^*. It is also apparent that $\Delta z^* q^* = 1$ at transport maxima. This is found to be a general property: transport maxima are always located on the hyperbola $\Delta z/H = 1$, in the region where $\Delta u > 0$ and the depth profiles are concave near the eastern wall. The maximum transport values are seen to approach 2 at small values of Δz^* (and correspondingly large values of q^*). This was to be expected, since for large q^*

$$Q_A^* \simeq \frac{1}{2q^{*2}} = \frac{1}{2}\Delta z^{*2} \tag{4.7}$$

at the points where $\Delta z/H = 1$. The ratio between (4.7) and the zero-PV detached flow expression (4.6) is exactly 2, showing that, for a given $\bar{B}$, transport in a flow with a finite, constant PV can be up to twice that predicted by zero-PV theory. Finally, it should be noted that the transports are always larger than, or of the order of, the zero-PV transports when $\Delta z^* q^* < 3/2$, and become significantly lower only for values of q^* that correspond to flows well inside the region with $\Delta z^* q^* > 3/2$ (i.e. the region of flows with negative Δu).

5. Discussion

We have shown in this work that Gill's semigeostrophic equations for rotating channel hydraulics can be exactly solved at the sill for a critical flow, once the sill height, the constant PV, and the average Bernoulli function $\bar{B}$ (i.e. the average flow energy) are prescribed. The choice of $\bar{B}$ as an upstream flow parameter has proven to be crucial: choosing a different flow invariant, such as the ψ_i parameter, used by Gill (1977) to partition the left and right boundary layer flows, or the Bernoulli function

on the eastern wall, used in Whitehead (2005), leads to high-order algebraic equations that are only amenable to numerical investigation. As noted by a referee, this choice may not be convenient from the observation point of view, since it requires that one measures B on both sidewalls. However, it has the great advantage of permitting an analytic characterization of attached critical flows at the sill section, and, in the case of detached flows, in the whole detached flow region. This choice also leads naturally to:

(i) the definition of a two-dimensional parameter space (the $(\Delta z^*, q^*)$ space of figure 2), in which properties of the critical flow solutions are easily assessed;

(ii) the derivation of simple, exact expressions for the critical mass fluxes, that directly extend the zero-PV formulae, and provide new insights into the effect of a finite PV on transport.

The results on transport, however, need to be further discussed in the context of previous work, since, at first sight, they appear to contrast with established results in the field. For example, the fact that transports can be up to twice those of the zero-PV theory seems to contradict the bound on transport of Killworth & McDonald (1993, referred to as KM hereafter), which in our context is

$$Q \leqslant \frac{g}{2f}\left(\frac{B_m}{g} - b_c\right)^2 \equiv Q_{KM}, \tag{5.1}$$

with B_m the maximum of B along streamlines that connect to the upstream basin. As noted in Pratt (2004), this result may be linked to the zero-PV theory as follows. Given a flow with an arbitrary B, one can pick the maximum value B_m and ask what the transport would be for a zero-PV flow with $B = B_m$, and depth vanishing at the western wall. According to (4.6), this transport is exactly given by (5.1). Thus, for given B_m, the zero-PV case does set a bound on finite-PV transport. On the other hand, if we compare flows with the same $\bar{B}$, (5.1) will give a larger bound when the PV is finite, since in this case B is non-constant, and $B_m > \bar{B}$. Due to the quadratic dependence of the KM bound on B_m, a moderate ratio $B_m/\bar{B}$ could be sufficient to give a significant increase in transport with respect to the zero-PV case, consistently with the findings of the previous section. To be more definite, consider the quantity

$$Q_e \equiv \frac{g}{2f}\left(\frac{B^-}{g} - b_c\right)^2, \tag{5.2}$$

obtained by replacing B_m with B^- in (5.1). Clearly, $Q_e \leqslant Q_{KM}$. Using the fact that $B^- - \bar{B} = qQ/2$ and the definitions of Δz^* and $q*$, and normalizing Q_e as in (4.2), yields

$$Q_e^* = \tfrac{1}{4}\left(q^* Q^* + \Delta z^*\right)^2. \tag{5.3}$$

It immediately follows from (5.3) that

$$Q_e^* - Q^* = \tfrac{1}{4}\left(q^* Q^* - \Delta z^*\right)^2 + (q^* \Delta z^* - 1)Q^*, \tag{5.4}$$

showing that $Q_e^* > Q^*$ at the transport maxima, and, *a fortiori*, for larger values of q^*. Direct computation of Q_e^*, for the values of Δz^* of figure 4, shows that the bound holds for any value of q^* (values of Q_e^*/Q_{0D}^* for the case $\Delta z^* = 1/4$ are shown as crosses in figure 4). This gives us sufficient confidence that our conclusions on transport are consistent with the KM bound, as they should be.

Another aspect of our results that appears to contradict common belief is the fact that maximum transport, for a given Δz, is achieved at finite PV. Even in this case, however, the contradiction is only apparent. Let us consider, for example, the results of some recent works by Whitehead and collaborators (WS; Whitehead 2005), in

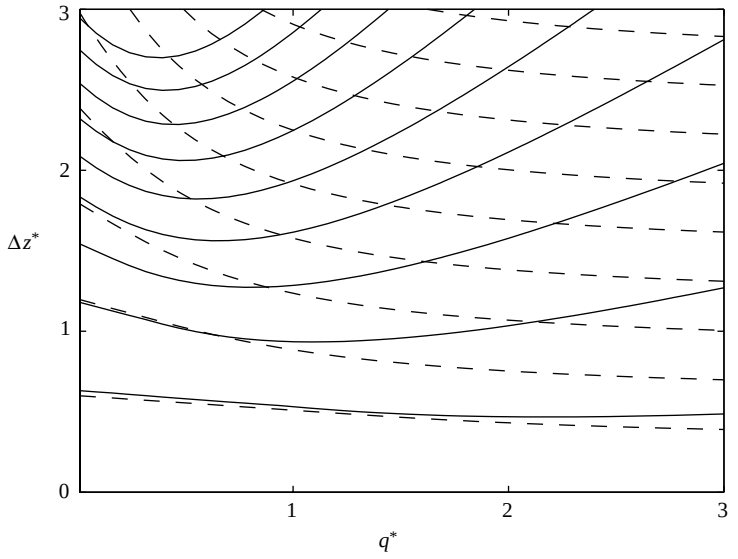

FIGURE 5. Contour lines of the normalized transport Q^* (solid lines), and of $\Delta z^*_W = \Delta z^* + q^* Q^*$ (dashed lines), in the normalized energy–PV space (Q^* increases in the positive Δz^* direction). For a given channel geometry, and given values of f and g, the contours of constant Δz^*_W are also contours of constant B^- (the Bernoulli function at the right-hand wall). Note that the transport decreases monotonically along these contours, in agreement with the findings of Whitehead & Salzig (2001) and Whitehead (2005).

which B^- is specified as one of the upstream flow parameters. It is shown in these works (see e.g. figure 4 of WS), that for a given value of B^- (or of closely related quantities), the transport is a decreasing function of the PV. How does this result compare with our figure 4? The answer is given in figure 5, which shows contour lines of the normalized transport Q^*, and of a parameter

$$\Delta z^*_W \equiv \Delta z^* + q^* Q^*, \tag{5.5}$$

in the plane $(\Delta z^*, q^*)$. The parameter Δz^*_W, used in Whitehead (2005), is obtained by replacing $\bar{B}$ by B^- in the definition of Δz. Therefore, for given geometrical parameters, contours of constant Δz^*_W are also contours of constant B^-, and, because of (5.3), of constant Q^*_e. It is seen from the figure that these contours always cross the contours of constant Q^* with a negative slope. Since Q^* is an increasing function of Δz^*, it follows that the transport along lines of constant Δz^*_W is a monotonically decreasing function of the PV, in agreement with the results of Whitehead and collaborators. On the other hand, it is clear from figure 5 that, for fixed Δz^*, the mass transport is a non-monotonic function of the PV: it first increases and then decreases with q, in agreement with figure 4. The key point, again, is the choice of the upstream invariants: since the relation between these quantities (Δz, Δz_W, Gill's ψ_i, etc.) involves the PV, it is to be expected that different choices may produce different dependences of transport on PV.

The previous results suggest that finite-PV may affect the estimates of transport in real oceanic straits more than it is commonly thought. This could be relevant to the outflows examined in Whitehead (1989) (Denmark Strait, Iceland-Faroe Channel, Ceara Rise, and Vema Channel), that have small values of Δz^*. Previous works on these straits have mostly concentrated on the effect of the topography representation, which is certainly crucial. An example is the work by Killworth (1992), that used

parabolic, or V-shaped sills, to improve on the original calculations by Whitehead (1989), based on a rectangular sill, which largely overestimated the observed fluxes (see e.g. table 1 in Pratt 2004). In two cases (Denmark Strait, Iceland-Faroe Channel), however, Killworth's corrections lead to values of transport considerably smaller than the observed ones. This raises the possibility that for these straits, taking both the sill topography and finite PV into account might lead to better agreement with the observations. A recent work by Nikolopoulos *et al.* (2003) on the Denmark Strait overflow seems to suggest that the inclusion of a finite, constant PV only leads to small changes of the mass flux, with respect to the estimate based on the zero-PV theory. This result, however, relies on solving the semigeostrophic equations for a single value of the PV, and appears to leave room for further work on the subject.

It is a pleasure to thank Peter Killworth, Jack Whitehead, and Andrea Bargagli for useful discussions. Insightful comments and suggestions by the referees are gratefully acknowledged.

Appendix

In the detached flow region, $\bar{h}$ is constant and (2.6) becomes a relation between $T(x)$ and the topography height $b(x)$,

$$\left(T^2 - T_c^2\right)^2 = 2T^2\left(1 + T_c^2\right)^2 \frac{\Delta b}{H}, \tag{A 1}$$

where $\Delta b \equiv b_c - b(x)$, and we have used (3.7)–(3.8), together with $h^+ = 0$. Let us now evaluate (A 1) at the point $x = x_s$, inside the obstacle range, where the flow separates from the western wall. At $x = x_s$, $T = T(w) \equiv T_w$, and (A 1) can be rewritten as

$$\frac{T_c^2}{1 + T_c^2} = \left(1 - \sqrt{\frac{2}{T_w^2}\frac{\Delta b(x_s)}{H}}\right)\frac{T_w^2}{1 + T_w^2} \equiv \alpha \frac{T_w^2}{1 + T_w^2}. \tag{A 2}$$

Clearly, $\alpha \leqslant 1$, the equality holding when the flow exactly separates at the sill. It follows from (A 2) that α and T_c monotonically decrease if the separation point moves upstream. Moreover, if

$$\delta \equiv \frac{b_c}{(H/2)\, T_w^2} > 1, \tag{A 3}$$

they will both vanish for some value of x_s within the obstacle range. Since the vanishing of T_c implies that of Δz, this means that when (A 3) is satisfied, the entire region below $C1$ in figure 2 is accessible. However, separation can only occur in a limited range of upstream values of x, whose precise size will depend on the actual shape of the obstacle. Clearly, if $\delta \gg 1$, the separation point will remain close to the critical section, no matter what the shape of the sill is. If, on the other hand, $\delta < 1$, separation can occur, in principle, at any x inside the obstacle range. In this case, however, T_c, and consequently $\Delta z/H$, will have non-zero minimum values, attained when $\alpha = 1 - \delta^{1/2}$ (i.e. when the separation occurs exactly at the left margin of the obstacle). Consequently, for a given q^*, there will be a limited range of values of Δz^* in which separated solutions are possible. This range, normalized by its maximum possible value, is readily computed as

$$R = \delta^{1/2}\frac{2 + \delta^{1/2} T_w^2}{2 + T_w^2}. \tag{A 4}$$

Note that $R \simeq 1$ if $\delta \simeq 1$. On the other hand, for small values of δ, $R \simeq \delta^{1/2}$, and the region of the parameter space available to separated flow solutions is strongly reduced. Using the definitions of H and q^*, δ can be rewritten as follows:

$$\delta = \frac{q^*}{(\tanh \sqrt{q^*})^2} \frac{b_c}{f^2 w^2/(2g)}. \tag{A 5}$$

In the small-PV limit, which is relevant to the experiments by WLK and to some of the experiments by Shen (1981), the dependence on q^* approximately cancels out in (A 5), and the range R becomes approximately proportional to $1/f$. Thus, increasing f progressively, as it is typically done in the experiments, would progressively reduce the range in Δz^* in which separated solutions can be found. In such a situation, accessing the region of detached flow solutions could require a fine tuning of the parameters, that may be difficult to realize experimentally. This raises the possibility that, in some cases, the inability to obtain separated flow solutions could be consequence of an insufficient control on the path followed by the experiment in the $(\Delta z^*, q^*)$-plane. Whether this applies to the cited laboratory experiments is difficult to judge, but seems worth further investigation.

REFERENCES

Borenäs, K. M. & Pratt, L. J. 1994 On the use of rotating hydraulics models. *J. Phys. Oceanogr.* **24**, 108–123.

Gill, A. E. 1977 The hydraulics of rotating-channel flow. *J. Fluid Mech.* **80**, 641–671.

Helfrich, K. R. & Pratt, L. J. 2003 Rotating hydraulics and upstream basin circulation. *J. Phys. Oceanogr.* **33**, 1651–1663.

Killworth, P. D. 1992 Flow properties in rotating, stratified hydraulics. *J. Phys. Oceanogr.* **22**, 997–1017.

Killworth, P. D. & McDonald, R. 1993 Maximal reduced-gravity flux in rotating hydraulics. *Geophys. Astrophys. Fluid Dyn.* **70**, 31–40.

Nikolopoulos, A., Borenäs, K., Hietala, R. & Lundberg, P. 2003 Hydraulic estimates of Denmark Strait overflow. *J. Geophys. Res.* **108**, Art. 3095.

Pratt, L. J. 1983 On inertial flow over topography. Part 1. Semigeostrophic adjustment to an obstacle. *J. Fluid Mech.* **131**, 195–218.

Pratt, L. J. 1987 Rotating shocks in a separated laboratory channel flow. *J. Phys. Oceanogr.* **17**, 483–491.

Pratt, L. J. 2004 Recent progress on understanding the effects of rotation in models of sea straits. *Deep-Sea Res.* II **51**, 351–369.

Pratt, L. J. & Armi, L. 1987 Hydraulic control of flows with nonuniform potential vorticity. *J. Phys. Oceanogr.* **17**, 2016–2029.

Pratt, L. J., Helfrich, K. R. & Chassignet, E. P. 2000 Hydraulic adjustment to an obstacle in a rotating channel. *J. Fluid Mech.* **404**, 117–149.

Shen, C. Y. 1981 The rotating hydraulics of open-channel flow between two basins. *J. Fluid Mech.* **112**, 161–188.

Whitehead, J. A. 1989 Internal hydraulic control in rotating fluids – applications to oceans. *Geophys. Fluid Dyn.* **48**, 169–192.

Whitehead, J. A. 1998 Topographic control of oceanic flows in deep passages and straits. *Rev. Geophys.* **36**, 423–440.

Whitehead, J. A. 2005 The effect of potential vorticity on flow rate through a gap. *J. Geophys. Res.* **110**, Art. C07007.

Whitehead, J. A., Leetmaa, A. & Knox, R. A. 1974 Rotating hydraulics of strait and sill flows. *Geophys. Fluid Dyn.* **6**, 101–125.

Whitehead, J. A. & Salzig, J. 2001 Rotating channel flow: control and upstream currents. *Geophys. Fluid Dyn.* **95**, 185–226.